Adhesion of Bacterial Exopolymers to α-FeOOH: Inner-Sphere Complexation of Phosphodiester Groups

Anselm Omoike,† Jon Chorover,*,† Kideok D. Kwon,‡ and James D. Kubicki‡

Department of Soil, Water and Environmental Science, The University of Arizona, Tucson, Arizona 85721, and Department of Geosciences, The Pennsylvania State University, University Park, Pennsylvania 16802

Received June 7, 2004. In Final Form: September 13, 2004

Extracellular polymeric substances (EPS) constitute a heterogeneous mixture of polyelectrolytes that mediate biomineralization and bacterial adhesion and stabilize biofilm matrixes in natural and artificial environments. Although nucleic acids are exuded extracellularly and are purported to be required for biofilm formation, direct evidence of the active mechanism is lacking. EPS were extracted from both *Bacillus subtilis* (a gram-positive bacterium) and *Pseudomonas aeruginosa* (a gram-negative bacterium) and their interaction with the goethite (α-FeOOH) surface was studied using attenuated total internal reflection infrared spectroscopy. Correspondence between spectral data and quantum chemical calculations demonstrate that phosphodiester groups of nucleic acids mediate the binding of EPS to mineral surfaces. Our data indicate that these groups emerge from the EPS mixture to form monodentate complexes with Fe centers on the goethite (α-FeOOH) surface, providing an energetically stable bond for further EPS or cell adhesion.

1. Introduction

Natural aquatic systems consist of complex assemblages of organic macromolecules (natural organic matter [NOM], bacterial exudates), inorganic colloids (clay minerals and oxides), and microbial cells. Mutual interactions among these constituents are important determinants of particle surface chemistry. For example, several studies have shown that adsorption of NOM to iron oxide particles alters their surface functionality, charge, and reactivity.[1−5] Bacterial cells also adhere to solid surfaces, such as Fe oxides, during incipient formation of biofilms,[6−7] thereby influencing not only solute mobility through sorption and precipitation processes[8−10] but also cell transport in the environment.[11]

Growth of a wide variety of gram-positive and gram-negative bacteria is accompanied by the production of extracellular polymeric substances (EPS) as capsule-like structures attached to cell envelopes (i.e., capsular or *cell-bound* EPS) or as slime polymers released into solution (*free* EPS). EPS are released as a hydrated matrix in biofilms (*biofilm* EPS) during the rapid colonization of abiotic surfaces in contact with water. EPS have been shown to contribute to biomineralization of iron oxyhydroxide (FeOOH), which may enhance metabolic energy generation by bacteria.[12] However, the molecular mechanisms of EPS−mineral interaction remain poorly resolved.

EPS are a complex mixture of biomacromolecules consisting primarily of polysaccharides and proteins, with variable but smaller amounts of lipids and nucleic acids.[13] These constituents contain neutral moieties (e.g., saccharide units), in addition to carboxyl, phosphate, and amino groups that ionize as a function of solution pH, of which any may serve as active sites for interaction with environmental surfaces.[14,15] Molecular mechanisms of adhesion between bacterial EPS and mineral surfaces include hydrophobic, electrostatic, covalent, and polymer−polymer interactions.[16,17] Although EPS mediates bacterial cell adhesion to minerals[18−20] and plays a vital role in biofilm formation,[21−23] the functional role of individual biomolecular groups is unclear.

The nucleic acid constituent of EPS can be a product of cell lysis.[24] However, it is well documented that diverse strains of bacteria, including viable *Bacillus* (gram positive) and *Pseudomonas* (gram negative) species, synthesize nucleic acids that are exuded into the environment.[25,26]

* Author to whom correspondence should be addressed. E-mail: Chorover@cals.arizona.edu.

† The University of Arizona.

‡ The Pennsylvania State University.

(1) Day, G. M.; Hart, B. T.; McKelvie, I. D.; Beckett, R. *Colloids Surf., A* **1994**, *89*, 1.

(2) Davis, J. A. *Geochim. Cosmochim. Acta* **1982**, *46*, 2381.

(3) Chorover, J.; Sposito, G. *Geochim. Cosmochim. Acta* **1995**, *59*, 875.

(4) Tippings, E.; Cooke, D. *Geochim. Cosmochim. Acta* **1982**, *46*, 75.

(5) Hunter, K. A.; Liss, P. S. *Nature* **1979**, *282*, 823.

(6) Marshall, K. C. In *Bacteria Adhesion*; Savage, D. C., Fletcher, M., Eds.; Plenum Press: London, 1985; pp 133−161.

(7) Marshall, K. C. In *Microbial Cell Surface Analysis; Structural and Physicochemical Methods*, Mozes, N., Handley, P. S., Busscher, H. J., Rouxhet, P. G., Eds.; VCH Publishers: New York, 1991; pp 3−19.

(8) Lee, J.; Beveridge, T. *Chem. Geol.* **2001**, *180*, 67.

(9) Ghiorse, M. C. *Annu. Rev. Microbiol.* **1984**, *38*, 518.

(10) Liehr, S. K. *Water Sci. Technol.* **1995**, *32*, 179.

(11) Appenzeller, B. M.; Duval Y. B.; Thomas, F.; Block. J. C. *Environ. Sci. Technol.* **2002**, *36*, 646.

(12) Chan, C. S.; Stasio, G. D.; Welch, S. A.; Girasole, M.; Frazer, B. H.; Nesterova, M. V.; Fakra, S.; Banfield, J. F. *Science* **2004**, *303*, 1656.

(13) Wingender, J.; Neu, T. R.; Flemming, H. C., Eds. *Microbial Extracellular Polymeric Substances: Characterization*, *Structure and Function*; Springer: Berlin, 1999.

(14) Beveridge, T. J.; Fyfe, W. S. *Can. J. Earth Sci.* **1985**, *22*, 1893.

(15) Beveridge, T. J. In *Bacteria in Nature*; Poindexter, J. S., Leadbetter, E. R., Eds.; Plenum: New York, 1989.

(16) van der Mei, H. C.; Meijer, S.; Busscher, H. J. *J. Colloid Interface Sci.* **1998**, *205*, 185.

(17) Tsuneda, S.; Aikawa, H.; Hayashi, H.; Yuasa, A.; Hirata, A. *FEMS Microbiol. Lett.* **2003**, *223*, 287.

(18) Gehrke, T.; Hallmann, R.; Sand. W. In *Biohydrometallurgical Processing*; Jerez, C. A., Vargas, T., Toledo, H., Wiertz, J. V., Eds.; University of Chile: Santiago, 1995; Vol. 1.

(19) Van der Aa, B. C.; Dufrene, Y. F. *Colloids Surf., B* **2002**, *23*,173.

(20) Pogliani, C.; Donati, E. *J. Ind. Microbiol. Biotech.* **1999**, *22*, 88.

(21) Fletcher, M.; Floodgate, G. D. *J. Gen. Microbiol.* **1973**, *74*, 325.

(22) Hseih, K. M.; Lion, L. W.; Shuler, M. L. *Biotech. Lett.* **1990**, *12*, 449.

(23) Lappin-Scott H. M.; Costerson, J. W. *Biofouling* **1989**, *1*, 323.

(24) Sutherland, I. W. *Trends Microbiol*. **2001**, *9*, 222.

10.1021/la048597+ CCC: $27.50
Published on Web 11/04/2004

Recent work indicates that nucleic acid exudates are required for the initial development of *P. aeruginosa* biofilms,[27] but the reason is not known. Molecular-scale methods are, therefore, required to elucidate the nature of interacting EPS and environmental media.

Fourier transform infrared (FTIR) spectroscopy is a powerful probe of molecular-scale organic−mineral binding interactions in complex systems. For example, prior FTIR studies have indicated that inner-sphere complexation of NOM carboxyl groups with Fe metal centers of hydrous oxide surfaces proceeds via a ligand-exchange mechanism.[28−32] The use of attenuated total reflectance (ATR) FTIR spectroscopy permits the acquisition of spectral data on hydrated samples (i.e., adsorbent in contact with aqueous solution) and in real time to elucidate adsorption mechanisms in situ.[30−33] In the ATR technique, internal reflectance of IR radiation in an internal reflective element (IRE) creates an evanescent wave that probes about 1 μm beyond the surface of the crystal into samples placed in close contact with it.

We used attenuated total reflectance Fourier transform infrared (ATR-FTIR) spectroscopy to investigate in situ (i.e., in the presence of water) and nondestructively (within the heterogeneous matrix of EPS) the nature of the interaction between EPS from gram-positive *B. subtilis* (ATCC 7003) and gram-negative *P. aeruginosa* (PAO1) and an iron oxide-coated Ge IRE at pH 6 in 10-mM NaCl. Quantum chemical calculations were employed to complement the experimental data and to elucidate the binding mechanism. Our results indicate that direct bonding of nucleic acid phosphodiester groups to Fe metal centers of iron oxides via monodentate complex formation may contribute significantly to bacterial adhesion at such surfaces.

2. Experimental Procedures

2.1. Materials. All chemicals were of analytical grade and were used without further purification. Ultrapure water (18 MΩ cm) was obtained from a Barnstead Thermolyne NANOpure Diamond UV water system (Dubuque, IA) and purged with ultrahigh purity N_2 prior to use.

2.2. Goethite (α-FeOOH) Synthesis and Characterization. The colloidal goethite used in this study was synthesized from $Fe(NO_3)_3$ by the method of Atkinson et al.[34] Sample characterization by X-ray powder diffraction (Philips X'pert MPD) and diffuse reflectance FTIR spectroscopy (Nicolet Magna 560 IR spectrometer) confirmed the formation of α-FeOOH. Particles were washed free of residual nitrate and freeze-dried prior to use. The goethite specific surface area (measured by N_2-BET) was 44.4 $m^2\,g^{-1}$. Transmission electron microscopy (TEM) showed that the particles are acicular and approximately 500 nm long. A stock suspension of goethite (25 g L^{-1}) was prepared using N_2-purged ultrapure water and the suspension was re-dispersed prior to each use.

2.3. EPS Isolation and Purification. *Bacillus subtilis* (ATTC 7003) and *Pseudomonas aeruginosa* (PAO1) were grown aerobically at 30 °C on Luria broth to early stationary growth phase (24 h). Cells were harvested by centrifugation (5000 g, 15 min, 4 °C), and EPS were isolated from the supernatant solution as described previously.[35] Briefly, the protocol involves recentrifugation of the supernatant solutions (12 000 g, 30 min, 4 °C) to remove residual cells followed by gradual precipitation of the EPS using three volumes of cold ethanol (4 °C). The suspension was then stored for 18 h at −20 ° C. The precipitated EPS were recovered by centrifugation (12 000 g, 30 min, 4 °C) and dialyzed against ultrapure water using Spectra/Por 7 Regenerated Cellulose (RC) membranes (1000 MWCO from Spectrum) to remove ethanol. After dialysis, for 72 h against two changes of water per day, the solution was freeze-dried and stored at −20 °C until use.

2.4. Coating of Germanium Crystal and FTIR Measurements. ATR-FTIR spectra were obtained on (i) solution-phase and (ii) goethite-sorbed EPS. All spectra were ratioed against that of the clean Ge IRE alone. The iron oxide-coated Ge IRE was prepared by spreading a colloidal goethite (α-FeOOH) suspension (0.5 mL of 25 g L^{-1} stock, pH 6 and 10 mM NaCl) onto the IRE and drying the coating in a vacuum oven for 19 h. A 0.5-mL aliquot of background electrolyte was added to the dried iron oxide film and carefully drained in order to remove loosely adhered goethite particles, rehydrate the oxide film, and prevent protein denaturation at the air/water interface. Spectra of the hydrated oxide were obtained. A clean Ge IRE crystal was exposed to EPS (0.5 mL; 17.9 mg mL^{-1}, pH 6 and 10 mM NaCl) in the presence and absence of the goethite coating. The progress of the interaction was monitored for 300 min at 22 ± 1 °C using a Nicolet Magna 560 FTIR spectrometer with a trough-style sample holder and Ge IRE (70 mm × 10 mm× 3 mm) subjected to a nominal incident beam angle of 45°, yielding 12 internal reflections at the sample surface. The spectrometer was continuously purged with CO_2-free air to eliminate CO_2 absorbances. A volatile liquid cover was used to prevent solution evaporation. All spectra were acquired at 4.0 cm^{-1} resolution with 350−500 scans. Difference spectra of adsorbed EPS were obtained by subtracting the spectrum of the hydrated goethite films from those of the hydrated goethite−EPS complexes. Spectra for solution-phase EPS were obtained using the same method, but with the bare Ge IRE only, uncoated by colloidal α-FeOOH.

2.5. Quantum Chemical Calculations. Nucleic acids are linked covalently by acidic phosphodiester groups at the 5′ and 3′ positions of the sugar moieties making them anionic at pH > 3.2.[36] Assuming a double helix nucleic acid structure, these phosphodiester groups are hypothesized to undergo ligand exchange with protonated hydroxyl groups attached to Fe metal centers on the oxide surface. Thus, in our molecular modeling, we employed deoxyribose phosphodiester ($PO_2(C_5O_3H_9)_2$), where the bases are omitted and replaced with H atoms on deoxyribose rings (Scheme 1). Bases of nucleic acids are presumed to be less important in binding to iron hydroxides, and the bases will little affect vibrational frequencies of the phosphodiester. This replacement saved significant computation time.

Quantum chemical calculations were performed using Gaussian 98[37] for the modeled deoxyribose phosphodiester clusters. Structures of modeled clusters (Figure 1) were energy minimized without any constraints, and IR frequencies were calculated with hybrid B3LYP functionals[38,39] and 6-31G(d)[40] basis set. Calculated

(25) Demain, M. H.; Burg, R. W.; Hendlin, D. *J. Bacteriol*. **1965**, *89*, 640.
(26) Brown, M. R. W.; Scott-Foster, J. H.; Clamp, J. R. *Biochem. J*. **1969**, *112*, 521.
(27) Whitchurch, C. B.; Tolker-Nielsen, T.; Ragas, P. C.; Mattick, J. S. *Science* **2002**, *295*, 1487.
(28) Kaiser, K.; Guggenberger, G.; Haumaier, L.; Zech, W. *Eur. J. Soil Sci.* **1997**, *8*, 301.
(29) Chorover, J.; Amistadi, M. K. *Geochim. Cosmochim. Acta* **2001**, *65*, 95.
(30) Gu, B. Schmitt, J.; Chen, Z.; Liyuan, L.; McCarthy, J. F. *Environ. Sci. Technol.* **1994**, *28*, 36.
(31) Gu, B. Schmitt, J.; Chen, Z.; Liyuan, L.; McCarthy, J. F. *Geochim. Cosmochim. Acta* **1995**, *59*, 219.
(32) Kubicki, J. D.; Itoh, M. J.; Schroeter, L. M.; Apitz, S. E. *Environ. Sci. Technol*. **1997**, *31*, 1151.
(33) Moulton, S. E.; Barisci, J. N.; McQuillan, A. J.; Wallace, G. G. *Colloids Surf., A* **2003**, *220*, 159.
(34) Atkinson, R. T.; Posner, A. M.; Quirk, J. P. *J. Phys. Chem.* **1967**, *71*, 550.
(35) Omoike, A.; Chorover, J. *Biomacromolecules* **2004**, *5*, 1219.
(36) Martinez, D. S.; Smith, R. E.; Kulczycki, E.; Ferris, F. G. *J. Colloid Interface Sci*. **2002**, *253*, 130.
(37) Frisch, M. J.; Trucks, G. W.; Schlegel, H. B.; Scuseria, G. E.; Robb, M. A.; Cheeseman, J. R.; Zakrzewski, V. G.; Montgomery, J. A., Jr.; Stratmann, R. E.; Burant, J. C.; Dapprich, S.; Millam, J. M.; Daniels, A. D.; Kudin, K. N.; Strain, M. C.; Farkas, O.; Tomasi, J.; Barone, V.; Cossi, M.; Cammi, R.; Mennucci, B.; Pomelli, C.; Adamo, C.; Clifford, S.; Ochterski, J.; Petersson, G. A.; Ayala, P. Y.; Cui, Q.; Morokuma, K.; Malick, D. K.; Rabuck, A. D.; Raghavachari, K.; Foresman, J. B.; Cioslowski, J.; Ortiz, J. V.; Stefanov, B. B.; Liu, G.; Liashenko, A.; Piskorz, P.; Komaromi, I.; Gomperts, R.; Martin, R. L.; Fox, D. J.; Keith, T.; Al-Laham, M. A.; Peng, C. Y.; Nanayakkara, A.; Gonzalez, C.; Challacombe, M.; Gill, P. M. W.; Johnson, B. G.; Chen, W.; Wong, M. W.; Andres, J. L.; Head-Gordon, M.; Replogle, E. S.; Pople, J. A. *Gaussian 98*, revision A.6; Gaussian, Inc.: Pittsburgh, PA, 1998.

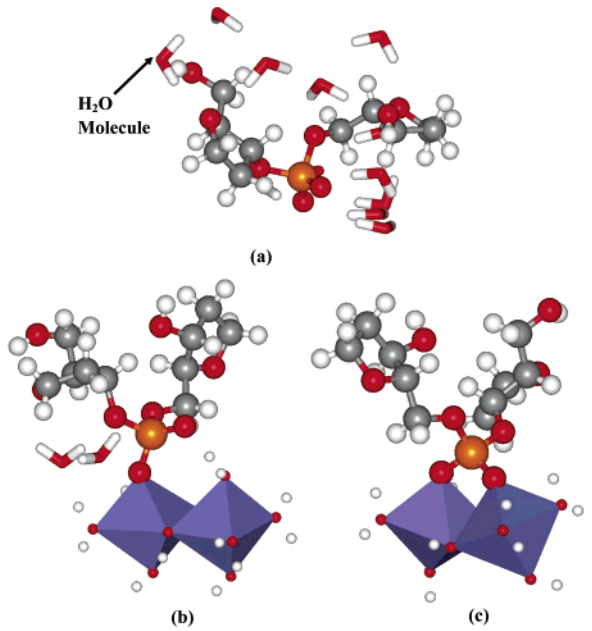

Figure 1. Optimized structures of deoxyribose phosphodiester and its surface complexes with iron cluster: (a) $PO_2(C_5O_3H_9)_2 \cdot (H_2O)_{12}$, a hydrated deoxyribose phosphodiester; (b) $Fe_2(OH)_4(OH_2)_5 \cdot PO_2(C_5O_3H_9)_2 \cdot (H_2O)_2$, a monodentate structure; (c) $Fe_2(OH)_4(OH_2)_4 \cdot PO_2(C_5O_3H_9)_2$, a bidentate structure. Red, oxygen; white, hydrogen; orange, phosphorus; blue, iron octahedra.

Scheme 1

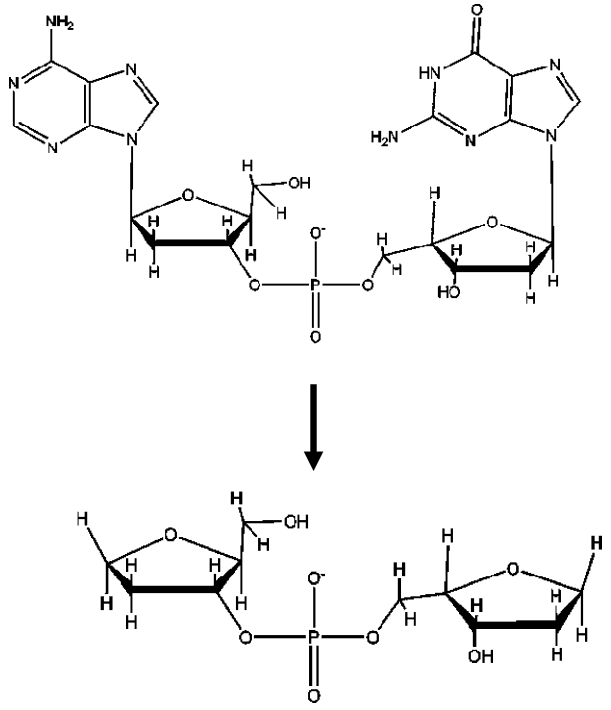

vibrational frequencies of orthophosphate Fe-hydroxide clusters using the same method[41] correlated well with experimental frequencies reported in the literature, and the good agreement validates the accuracy of the method used here.

H-bonding of H_2O molecules to anionic functionalities can change vibrational frequencies of the latter to a significant degree.[42] In this study, 12 H_2O molecules were added to the deoxyribose phosphodiester model (i.e., $PO_2(C_5O_3H_9)_2 \cdot (H_2O)_{12}$) in order to model the solvated state and obtain reliable frequencies (Figure 1a). The phosphodiester/Fe-hydroxide clusters were modeled to describe inner-sphere complexation of a nucleic acid with Fe-hydroxide surfaces. Both monodentate $[Fe_2(OH)_4(OH_2)_5 \cdot PO_2(C_5O_3H_9)_2 \cdot (H_2O)_2]$ (Figure 1b) and bidentate $[Fe_2(OH)_4(OH_2)_4 \cdot PO_2(C_5O_3H_9)_2]$ (Figure 1c) structures were included. We did not include explicit H_2O molecules in modeling the inner-sphere complexes because bridging oxygens are expected to be less sensitive to H-bonding than nonbridging oxygens (e.g., phosphate anions), and their inclusion would have increased dramatically the requisite computational time. However, two H_2O molecules were added in the monodentate structure because we found deformation of the Fe dimer due to interaction with the phosphodiester during the energy minimization. A minimum of two H_2O molecules were necessary to stabilize the Fe dimer, which represents the Fe-hydroxide surface, in the monodentate structure.

Frequencies based on the energy-minimized structures in a gas phase were scaled by a factor of 0.9614[43] to correct systematic errors such as neglect of anharmonicity and basis set size. Vibrational modes corresponding to calculated frequencies were analyzed and assigned using Molden (version 4.0).[44] Correlation analysis was performed for calculated versus experimental frequencies to determine which type of surface complex corresponds most closely to the experimental spectra. Reaction energies approximate to energies of adsorption from solution for phosphodiester were calculated using a solvent continuum method, Integral Equation Formalism Polarized Continuum

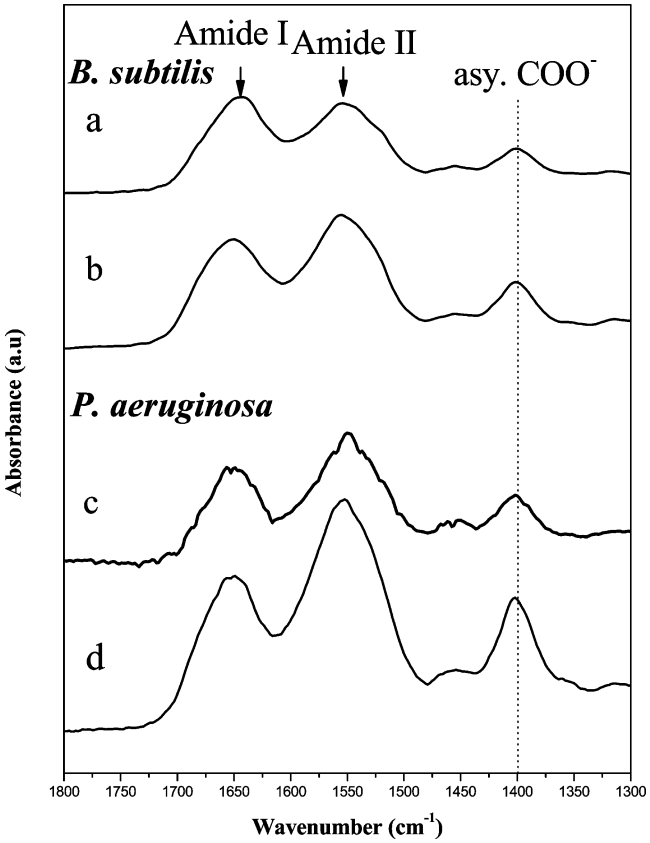

Figure 2. ATR−FTIR spectra (1800−1300 cm^{-1}) of solution-phase EPS and adsorbed EPS after 60 min reaction time: (a) *B. subtilis* EPS (free), (b) *B. subtilis* EPS after contact with goethite, (c) *P. aeruginosa* EPS (free), and (d) *P. aeruginosa* EPS after contact with goethite (17.9 mg mL^{-1} EPS solution, pH 6.0 and 10 mM NaCl).

(38) Becke, A. D. *J. Chem. Phys.* **1993**, *98*, 5648.
(39) Lee, C. T.; Yang, W. T.; Parr, R. G. *Phys. Rev. B* ***1988***, *37*, 78541.
(40) Hehre W. J.; Ditchfield, R.; Pople, J. A. *J. Chem. Phys.* **1972**, *56*, 2257.
(41) Kwon, K. D.; Kubicki, J. D. *Langmuir* **2004**, *20*, 9249.
(42) Kolmodin, K.; Luzhkov, V. B.; Åqvist, J. *J. Am. Chem. Soc.* **2002**, *124*, 10130.
(43) Scott, A. P.; Radom, L. *J. Phys. Chem.* **1996**, *100*, 16502.
(44) Schaftenaar, G.; Noordik, J. H. *J. Comput. Aided Mol. Des.* **2000**, *14*, 123.

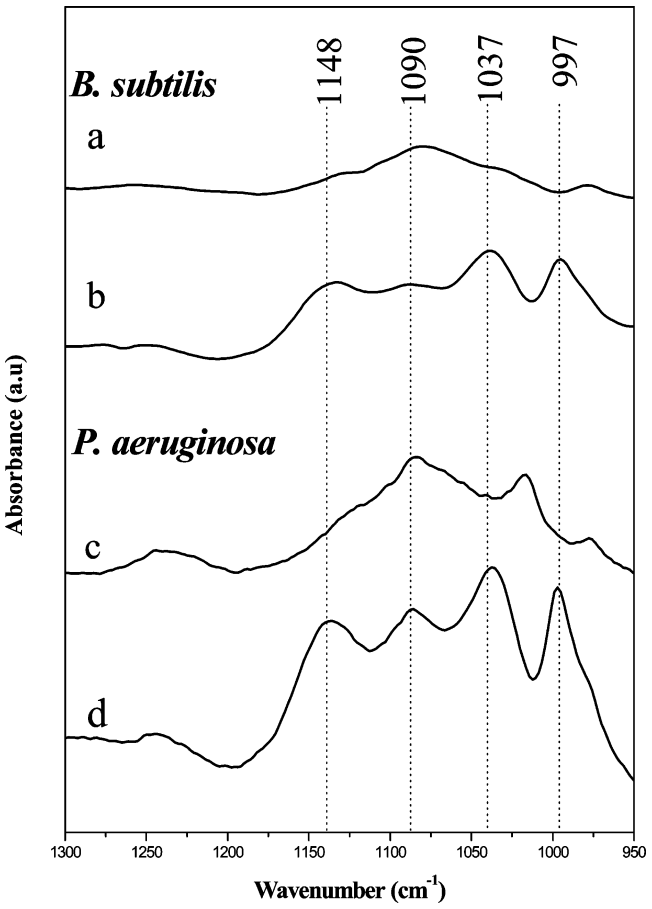

Figure 3. ATR−FTIR spectra (1300−950 cm^{-1}) of solution-phase EPS and adsorbed EPS after 60 min reaction time: (a) *B. subtilis* EPS (free), (b) *B. subtilis* EPS after contact with goethite, (c) *P. aeruginosa* EPS (free), and (d) *P. aeruginosa* EPS after contact with goethite (17.9 mg mL^{-1} EPS solution, pH 6.0 and 10 mM NaCl).

Model (IEFPCM)[45,46] and the B3LYP/6-311+G(d,p) method based on B3LYP/6-31G(d), with energy-minimized structures in the gas phase.

3. Results and Discussion

3.1. ATR-FTIR Spectra of EPS. Interaction with the goethite surface induces distinct changes in the ATR-FTIR spectra of EPS isolated from the early stationary phase (24 h) culture solution of *B. subtilis* and *P. aeruginosa*, particularly in the 1800−1300 cm^{-1} (Figure 2) and 1300−950 cm^{-1} (Figure 3) regions. The three bands of interest in the 1800−1300 region centered at 1643, 1556, and 1402 cm^{-1} are assigned to amide I (vibrations mainly from in-plane stretching of the C═O band of proteins), amide II (primarily N−H bending coupled to C−N stretching modes of proteins), and symmetrical C−O stretching of carboxylate (COO^-) in proteins, fatty acids, and uronic acids (Figure 2a). Amide bands are sensitive to protein structure. Amide I, in particular, is commonly used to elucidate secondary-structure changes of proteins.[47,48] In Figure 2a, the amide I band for solution-phase *B. subtilis* EPS, located at about 1643 cm^{-1}, is shifted to 1652 cm^{-1} and broadened in bandwidth after contact with the goethite surface (Figure 2b). In addition, the amide I/amide II band-intensity ratio is decreased. Similar effects were observed for *P. aeruginosa*; the amide I band is broadened, shifted from 1648 (Figure 2c) to 1657 cm^{-1} (Figure 2d) and the amide I/amide II intensity ratio is reduced. The amide I frequency shifts are consistent with protein conformational change from random or disordered structure (1660−1650 cm^{-1}) to α-helix structure (1650−1640 cm^{-1}),[49−51] indicating either change in protein conformation of EPS upon adsorption or preferential adsorption of protein constituents that differ in conformation from the bulk. It is important to note that interaction of EPS from *B. subtilis* and *P. aeruginosa* with goethite-coated IRE showed no noticeable change in the shape and peak position of the C═O stretching vibration of ionized carboxylate (COO^-), suggesting that these anionic groups did not form direct bonds with the goethite surface (Figure 2).

In the 1300−950 cm^{-1} region, distinct spectral changes due to EPS−goethite interaction were observed in all spectra (Figure 3). Absorption bands resulting from asymmetric stretching vibrations of phosphodiesters occur between 1250 and 1200 cm^{-1}, whereas the symmetric stretching vibrations at 1088−1084 cm^{-1} overlap with the complex sequence of bands between 1100 and 900 cm^{-1} arising from C−O, C−O−C, and C−O−P stretching modes of polysaccharides (sugar/sugar phosphate).[51] In the region 1100−950 cm^{-1}, solution-phase *B. subtilis* EPS (no goethite sorbent, Figure 3a) shows a broad band at 1080 cm^{-1} and a shoulder at 978 cm^{-1} and has significantly less structure compared to that of goethite-sorbed *B. subtilis* EPS (Figure 3b). After exposure of EPS solution to goethite, the emergence of four clear bands at 1148, 1090, 1037, and 997 cm^{-1} (Figure 3b) is attributable to stretching modes of P−OH and P−OFe bonds.[52,53] Identical bands were observed when EPS from *P. aeruginosa* were reacted with goethite (Figure 3c−d). In both cases, the reaction is relatively rapid; no significant difference was observed between 8 min and 1 h or longer reaction time.

In IR studies of methylphosphonic acid (MPA) on goethite, bands at ∼1015 and 984 cm^{-1} were assigned to asymmetric and symmetric stretching vibrations of P−OFe.[53] Frequency shift and intensity variation of the PO_2^- stretching at 1253, 1092, 1000, and 913 cm^{-1} were attributed to direct binding of Fe(III) to PO_2^- groups in adenosine-5′-triphosphate.[54] In addition, the presence of bands at 1232, 1158, and 1000 cm^{-1} in the difference spectrum for guanosine-5′-triphosphate were attributed to direct Fe−phosphate binding in the presence of Fe(II) chloride. We observe similar changes in EPS spectra during reaction with goethite, which is also consistent with inner-sphere Fe−phosphodiester complexation.

The structure of the phosphate−goethite bond is controversial even for simple systems comprising orthophosphate. Tejedor-Tejedor and Anderson[55] suggested that bands at 1123, 1006, and 982 cm^{-1} resulted from the protonated bidentate-binuclear surface complex, $\equiv Fe_2HPO_4$, whereas the bands located at 1096 and 1044 cm^{-1} were from the deprotonated bidentate-binuclear surface complex, $\equiv Fe_2PO_4^-$. In another study, Persson et al.[56]

(45) Cancès, E.; Mennucci, B.; Tomasi, J. *J. Chem. Phys.* **1997**, *107*, 3032.
(46) Cossi, M.; Scalmani, G.; Rega, N.; Barone, V. *J. Chem. Phys.* **2002**, *117*, 43.
(47) Haris, P. I.; Severcan, F. *J. Mol. Catal. B: Enzym.* **1999**, *7*, 207.
(48) Pelton, J. T.; McLean, L. R. *Anal. Biochem.* **2000**, *277*, 167.
(49) Susi, H.; Byler, D. M. *Biopolymers* **1986**, *25*, 469.
(50) Buijs, J.; Norde, W.; Lichtenbelt, J. W. Th. *Langmuir* **1996**, *12*, 1605.
(51) Naumann, D.; Schultz, C. P.; Helm D. In *Infrared Spectroscopy of Biomolecules*; Mantsch, H. H., Chapman, D., Eds.; Wiley-LISS: New York, 1996; pp 279−310.
(52) Sheals, J.; Sjoberg S.; Persson, P. *Environ. Sci. Technol.* **2002**, *36*, 3090.
(53) Barja, B. C.; Tejedor-Tejedor, M. I.; Anderson, M. A. *Langmuir* **1999**, *15*, 2316.
(54) el-Mahdaoui, L.; Tajmir-Riahi, H. A. *J. Biomol. Struct. Dyn.* **1995**, *13*, 69.
(55) Tejedor-Tejedor, M. I.; Anderson M. A. *Langmuir* **1999**, *15*, 602.

Table 1. Calculated Frequencies of Deoxyribose Phosphodiester Clusters and Experimental Frequencies of EPS on Goethite

calculated frequencies[b] (cm^{-1}) assignments[c]			experimental frequencies (cm^{-1})
phosphodiester in solution	monodentate cluster	bidentate cluster	[e]EPS on goethite
823 deoxyribose	941	901	937 (938)
909 deoxyribose	968	972	960 (976)
999 υ(RO−P−OR)	1009[d]	1014	997 (996)
	1025[d]		
1042[d] υ_s(=O−P−O$^=$)	1045 υ_s(FeO−PO$^=$)	1027 υ_s(FeO−P−OFe)	1037 (1034)
1050[d]			
	1067	1060[d]	1076 (1078)
		1076[d]	
	1102	1090 υ_{as}(FeO−P−OFe)	1090 (1086)
1205 υ_{as}(=O−P−O$^=$)	1176 υ_{as}(FeO−PO$^=$)		1148 (1150)

[a] Vibrational modes were assigned for the calculated frequencies, atomic motions of which are clear to define. [b] Calculated frequencies are presented after scaling. [c] Assignment symbols: υ_{as}, asymmetric stretching; υ_s, symmetric stretching; υ, stretching coupled with bending modes; O$^=$, nonbridging oxygen of phosphate; O, bridging oxygen of phosphate; R, deoxyribose ring. [d] Adjacent frequencies show almost identical vibrational modes. [e] Second derivative peak positions for *Bacillus subtilis* (*P. aeruginosa*) EPS.

Table 2. Energies (1 Hartree = 2625.5 kJ mol^{-1}) of Phosphodiester Species Calculated with IEFPCM[45,46] Using B3LYP/6-311+G(d,p)[a]

species	E_{Gas} ($/E_h$)	ΔG_{sol} (kJ mol^{-1})	$\langle\Psi_{final}\|H\|\Psi_{final}\rangle$ ($/E_h$)	$\Delta G_{sol} + \langle\Psi_{final}\|H\|\Psi_{final}\rangle$ ($/E_h$)
$[PO_2(C_5O_3H_9)_2(H_2O)_{12}]^{-1}$	−2253.22684	−91.46	−2253.22125	−2253.25609
$H_3O^+(H_2O)_4$	−382.40710	−245.56	−382.71436	−382.80788
$OH^-(H_2O)_4$	−381.55350	−231.84	−381.78316	−381.87147
$5H_2O$	−382.04110	−35.98	−382.34473	−382.35844
Surfaces				
$[Fe_2(OH)_5(OH_2)_5(H_2O)_4]^{1+}$	−3594.91765	−244.35	−3594.91203	−3595.00510
$[Fe_2(OH)_4(OH_2)_6(H_2O)_4]^{2+}$	−3595.21876	−647.52	−3595.21464	−3595.46127
Bidentate Complexes				
$[Fe_2(OH)_4(OH_2)_4]PO_2(C_5O_3H_9)_2$	−4472.13595	−272.09	−4472.12557	−4472.22917
Monodentate Complexes				
$[Fe_2(OH)_4(OH_2)_5]PO_2(C_5O_3H_9)_2(H_2O)_2$	−4701.56842	−244.05	−4701.55898	−4701.65193

[a] E_h = Hartree energy unit, ΔG_{sol} = electrostatic + nonelectrostatic solvation energy, $\langle\Psi_{final}|H|\Psi_{final}\rangle$ = internal energy of species in a continuum cavity.

refuted the formation of bidentate surface complexes in orthophosphate adsorption to goethite and assigned peaks at 1122 and 1049 cm^{-1} to monodentate complex formation. In the present work, molecular modeling was employed to confirm that our spectra indicate the inner-sphere complexation of EPS phosphodiester groups at surface Fe centers and to propose an accurate configuration for the resulting complex.

3.2. Quantum Chemical Calculations. *3.2.1. Geometries of Model Structures.* The P−O$^=$ (O$^=$: nonbridging oxygen) distances of the model aqueous deoxyribose phosphodiester (Figure 1a) were 1.51 Å. The P−O distances increased from 1.51 Å (P−O$^=$) to 1.53 and 1.54 Å (P−O_{Fe}, O_{Fe}: bridging oxygen connected to Fe) in the monodentate and bidentate model surface complexes, respectively (Figure 1b and c). In the monodentate complex, the other P−O$^=$ distance was 1.50 Å. However, the distance of P−O_C (O_C: bridging oxygen connected to sugar) decreased slightly from 1.64 and 1.67 Å to 1.62 and 1.63 Å (monodentate complex) and 1.59 and 1.60 Å (bidentate complex).

Distances of Fe−OP (between Fe and O_{Fe}) were 1.97 Å in the monodentate complex and 2.06 Å in the bidentate complex. However, the distance between P and Fe of the monodentate complex (3.39 Å) exceeded that of the bidentate complex (3.22 Å). These Fe−P distances are in the range of those measured by X-ray absorption spectroscopy of colloidal phosphate−iron complexes (3.05−3.39 Å)[57] and phosphate minerals such as vivianite (3.19−3.43 Å).[58] The bond angles of Fe−O−P reflect the difference in bond distances; the angle of the monodentate complex (151°) exceeds that of the bidentate complex (126 and 127°). Energy minimization with two Fe−O−P linkages leads to narrower Fe−O−P angles in the bidentate complex, which causes more distortion of the Fe−dimer structure (Figure 1c). Fe−Fe distances of both complexes were 3.03 Å; the Fe−Fe distance in goethite ranges from 3.015 to 3.39 Å.[59] These energy-minimized structures are reasonable from several perspectives discussed in more detail in sections 3.2.2−3.2.4. First, the calculations show that phosphodiester groups can indeed form covalent bonds to iron hydroxides (inner-sphere complexes). Second, the calculated frequencies of the monodentate structure are capable of accurately predicting the experimental spectroscopic data. Finally, the energy calculations predicted the same results as did the frequency calculations alone.

3.2.2. Frequency Calculation. The calculated frequencies of deoxyribose phosphodiester clusters are listed in Table 1, along with the experimental frequencies of goethite-sorbed EPS. The calculation shows that significant frequency shifts—relative to the model aqueous phosphodiester—are induced by inner-sphere complex formation. Frequencies of nonbridging oxygens of phosphates were downshifted after they became bridging oxygens due to bond formation with the Fe-hydroxide cluster. Shifts were

(56) Persson, P.; Nilsson, N.; Sjoberg, S. *J. Colloid Interface Sci.* **1996**, *177*, 263.

(57) Rose, J.; Flank, A. M.; Masion, A.; Bottero, J. Y.; Elmerich, P. *Langmuir* **1997**, *13*, 1827.

(58) Rose, J.; Manceau, A.; Bottero, J. Y.; Masion, A.; Garcia, F. *Langmuir* **1996**, *12*, 6701.

(59) Waychunas, G. A.; Fuller, C. C.; Rea, B. A.; Davis J. A. *Geochim. Cosmochim. Acta* **1996**, *60*, 1765.

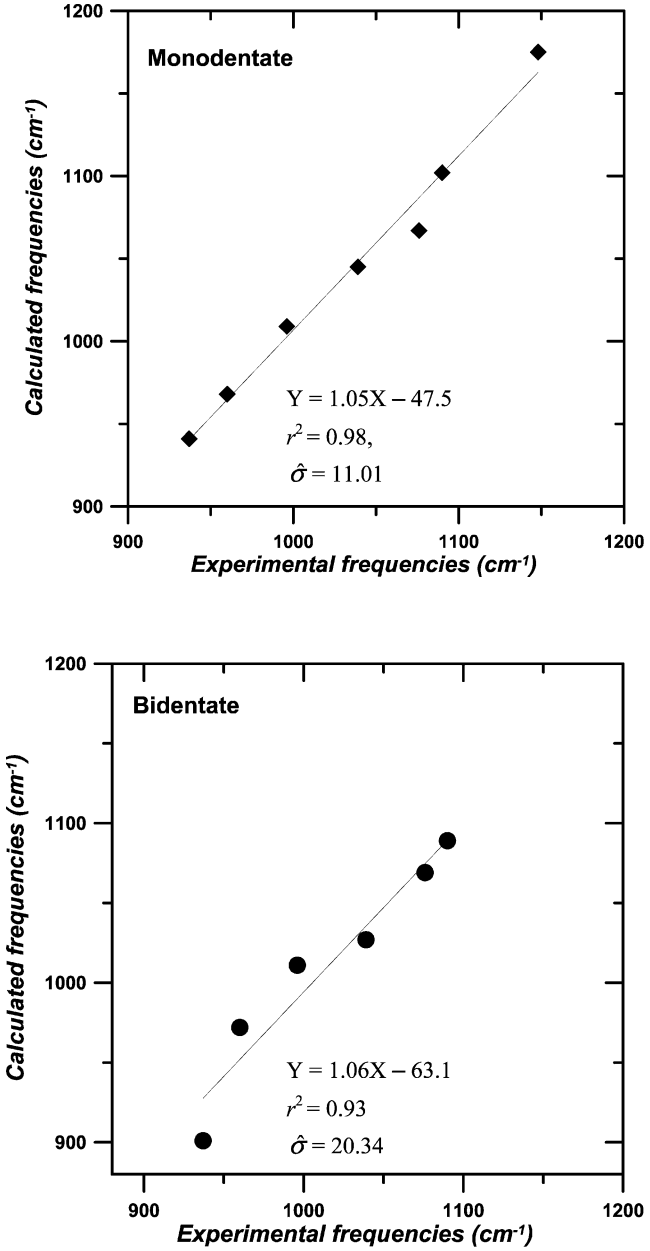

Figure 4. Correlation between calculated and experimental frequencies of the phosphodiester Fe-hydroxide clusters. The correlation was determined by linear regression: $Y = mX$, where Y = calculated frequency and X = experimental frequency, r^2 is a coefficient of determination, and $\hat{\sigma}$ is a root-mean-squared error in the linear regression analysis.

from 1205 and 1050 cm^{-1} (for nonbridging oxygens) to 1176 and 1045 cm^{-1} in the monodentate complex and to 1090 and 1027 cm^{-1} in the bidentate complex. The higher frequencies for the monodentate complex are due to the persistence of one nonbridging oxygen, relative to the bidentate case (Figure 1). The increase in bond distance for $P-O_{Fe}$ in going from monodentate to bidentate complexes may explain the higher frequencies of the monodentate complex.

3.2.3. Frequency Correlation. Analysis of correlation between experimental and calculated frequencies in the region of 1200−900 cm^{-1} was performed by linear regression (Figure 4). The calculated regression parameters (i.e., slopes, intercepts, determination coefficients, and root mean-squared errors) imply that the monodentate frequencies are more linearly correlated with experimental values than are the bidentate frequencies. That is, calculated frequencies of the monodentate structure more closely approximated experimental data than did those for the bidentate structure, for both gram-positive (*B. subtilus*) and gram-negative (*P. aeruginosa*) bacterial EPS sorbed to goethite. The better correlation for the monodentate complex is mainly caused by prediction of a band corresponding to the experimental frequency of 1148 cm^{-1}, which the bidentate cluster did not predict (Table 1).

The frequency calculations suggest that phosphodiesters of the bacterial EPS probably form monodentate, rather than bidentate, inner-sphere complexes on Fe-hydroxides. In addition, on the basis of the correlation and vibrational mode analyses, we suggest that the emergent peaks at 1148 and 1037 cm^{-1} observed in the ATR-FTIR experiments (Figure 3) correspond to asymmetric and symmetric stretching of $FeO-P-O^{=}$ upon goethite surface complexation of phosphodiester in EPS.

3.2.4. Reaction Energy Calculation. We also calculated relative reaction energies to approximate energies of adsorption for monodentate and bidentate surface complex formation. The reaction energies were calculated using B3LYP/6-311+G(d,p)//B3LYP/6-31G(d) with a combined solvation method[60] of implicit continuum solvation (IEF-PCM[45,46]) and explicit H_2O solvation. Because the Gibbs energy of a solute is not precisely defined in the continuum solvation method, we used a sum of solvation free energy (electrostatic and nonelectrostatic contributions associated with solvent) and internal energy of the final wave function for reaction energies (Table 2). This energy quantity is appropriate to determine favorable reactions; the cluster-type calculations produce many low frequencies,[61] which can lead to significant errors in entropy determination.[62] We used the summation energies listed in Table 2 to obtain the reaction energies indicated in Table 3.

We simulated possible reactions of phosphodiesters occurring at iron hydroxide surfaces around neutral pH. Iron hydroxides have slightly positive charge at neutral pH due to protonation of surface hydroxyls ($Fe-OH_2^+$), as predicted from isoelectric points of iron hydroxides (7.5−8.5).[63] The surface charge of α-FeOOH was modeled by controlling the number of H_2O and OH ligands bound to Fe centers of the iron dimer. The surface with a +2 charge was modeled as $[Fe_2(OH)_4(OH_2)_6(H_2O)_4]^{2+}$ and the surface with a +1 charge was modeled as $[Fe_2(OH)_5(OH_2)_5(H_2O)_4]^{1+}$. The surface functional groups were assumed to exchange with phosphodiester ligands, and Table 3 lists the possible reactions.

Use of surface complex structures can cause errors in calculation of absolute reaction energies because they do not comprise as many solvation H_2O molecules as the same phosphodiester in bulk solution. However, relative comparison of energetics associated with the different types of complexes will compensate for the error. Relative energy comparison shows that complexation energies are more negative at more positively charged surfaces (−6 to −26 kJ mol^{-1} on a +2 surface, and +75 to +55 kJ mol^{-1} on a +1 surface). Furthermore, monodentate complex formation is more favorable energetically than bidentate complex formation (by 20 kJ mol^{-1}). This is consistent with the frequency calculation, further supporting our assessment that it is monodentate rather than bidentate complex formation that gives rise to the experimental FTIR spectra.

(60) Chalmet, S.; Rinaldi, D.; Ruiz-Lopez, M. F. *Int. J. Quantum Chem.* **2001**, *84*, 559.
(61) Ayala, P. Y.; Schlegel, H. B. *J. Chem. Phys.* **1998**, *108*, 2314.
(62) Cramer, C. J. *Essentials of computational chemistry;* John Wiley & Sons Ltd: Chichester, 2003.
(63) Parks, G. A. *Chem. Rev.* **1965**, *65*, 177.

Table 3. Reactions Energies of Possible Phosphodiester Adsorptions to Positively Charged Fe-Hydroxides from Solution

Adsorption to (+2) Charged Surface, $[Fe_2(OH)_4(OH_2)_6(H_2O)_4]^{2+}$

bidentate $\Delta E = -6$ kJ mol^{-1}

$[PO_2(C_5O_3H_9)_2(H_2O)_{12}]^{-1} + [Fe_2(OH)_4(OH_2)_6(H_2O)_4]^{2+} \rightarrow [Fe_2(OH)_4(OH_2)_4]PO_2(C_5O_3H_9)_2 + 3.6[5(H_2O)]$

monodentate $\Delta E = -26$ kJ mol^{-1}

$[PO_2(C_5O_3H_9)_2(H_2O)_{12}]^{-1} + [Fe_2(OH)_4(OH_2)_6(H_2O)_4]^{2+} \rightarrow [Fe_2(OH)_4(OH_2)_5]PO_2(C_5O_3H_9)_2(H_2O)_2 + 3[5(H_2O)]$

Adsorption to (+1) Charged Surface, $[Fe_2(OH)_5(OH_2)_5(H_2O)_4]^{+}$

bidentate $\Delta E = +75$ kJ mol^{-1}

$[PO_2(C_5O_3H_9)_2(H_2O)_{12}]^{-1} + [Fe_2(OH)_5(OH_2)_5(H_2O)_4]^{+} \rightarrow [Fe_2(OH)_4(OH_2)_4]PO_2(C_5O_3H_9)_2 + [OH^{-}(H_2O)_4] + 2.6[5(H_2O)]$

monodentate $\Delta E = +55$ kJ mol^{-1}

$[PO_2(C_5O_3H_9)_2(H_2O)_{12}]^{-1} + [Fe_2(OH)_5(OH_2)_5(H_2O)_4]^{+} \rightarrow [Fe_2(OH)_4(OH_2)_5]PO_2(C_5O_3H_9)_2(H_2O)_2 + [OH^{-}(H_2O)_4] + 2[5(H_2O)]$

4. Conclusions

Infrared spectra of EPS from both gram-negative and gram-positive bacterial strains are consistent with P−O−Fe bond formation upon adsorption to the goethite surface. Molecular modeling facilitates the interpretation of IR experimental results in showing that phosphodiesters of EPS can form inner-sphere complexes on Fe-oxy(hydr)-oxides. Frequency calculations using deoxyribose phosphodiester clusters were employed to elucidate the nature of bonding interactions. Linear correlation of calculated versus experimental frequencies revealed better agreement for monodentate ($r^2 = 0.98$, $p < 0.001$) than for bidentate ($r^2 = 0.93$, $p < 0.001$) inner-sphere surface complexes that result from ligand exchange between the phosphodiester group and Fe surface hydroxyls. Reaction-energy calculations also indicated the favorability of monodentate over bidentate complex formation at positively charged sites of Fe hydroxide. Covalent bond formation between these extracellular biomolecules and Fe hydroxides may, therefore, provide a strong anchor for conditioning film formation, including subsequent adsorption of macromolecules with lower oxide affinity and adhesion of bacterial cells during incipient biofilm formation.

Acknowledgment. This research was supported by the National Science Foundation (NSF) CRAEMS program (Grant No. CHE-0089156). Computation was supported in part by the Materials Simulation Center, a Penn State MRSEC and MRI facility.

LA048597+